APL Materials

# Charge-transfer in B-site-depleted $NdGaO_3$/$SrTiO_3$ heterostructures

Cite as: APL Mater. **6**, 076104 (2018); https://doi.org/10.1063/1.5038773
Submitted: 05 May 2018 . Accepted: 02 July 2018 . Published Online: 23 July 2018

F. Gunkel, C. Lenser, C. Baeumer, F. Borgatti, F. Offi, G. Panaccione, and R. Dittmann

# Charge-transfer in B-site-depleted $NdGaO_3/SrTiO_3$ heterostructures

F. Gunkel,[1,2] C. Lenser,[3] C. Baeumer,[2,4] F. Borgatti,[5] F. Offi,[6]
G. Panaccione,[7] and R. Dittmann[2,4]
[1]*Institute of Electronic Materials (IWE2), RWTH Aachen University, Aachen, Germany*
[2]*Jülich-Aachen Research Alliance, Fundamentals of Future Information Technology (JARA-FIT), Aachen, Germany*
[3]*IEK-1, Forschungszentrum Jülich, 52425 Jülich, Germany*
[4]*Peter Grünberg Institute (PGI-7), Forschungszentrum Jülich, 52425 Jülich, Germany*
[5]*CNR–Istituto per lo Studio dei Materiali Nanostrutturati (ISMN), Via P. Gobetti 101, I-40129 Bologna, Italy*
[6]*CNISM and Dipartimento di Scienze, Università di Roma Tre, Via della Vasca Navale 84, 00146 Rome, Italy*
[7]*CNR–Istituto Officina dei Materiali (IOM), Laboratorio TASC, S.S. 14 Km 163.5, AREA Science Park, Basovizza, 34149 Trieste, Italy*

(Received 5 May 2018; accepted 2 July 2018; published online 23 July 2018)

Cation stoichiometry has been identified as a major key in establishing 2-dimensional electron gases (2DEGs) in oxide heterostructures. Here, we discuss a 2DEG formation scenario in B-site deficient perovskite/perovskite heterostructures, which previously were predicted to show insulating behavior. We elaborate an ionic picture based on oxygen-vacancy-buffered B-site vacancy defects in the polar oxide layer that yields a continuous transition from 2DEG formation to less conducting interfaces to insulating interfaces with increasing B-site deficiency. Experimentally, a corresponding modulation of charge transfer across $NdGaO_3/SrTiO_3$ interfaces is inferred using hard x-ray photoelectron spectroscopy analysis and transport experiments. With increasing B-site deficiency, we observe a decrease of the interfacial $Ti^{3+}$ core level contribution, indicating a reduced charge transfer at the interface. This result is corroborated by temperature-dependent transport measurements, revealing increased low temperature resistance, with a dominant influence of a reduced electron density in the Ga-depleted sample. We consider a redistribution of oxygen vacancies in the B-site deficient polar oxide layer to explain the alleviated interface reconstruction, adding a new perspective on potential built-up in polar-oxide thin films. 
https://doi.org/10.1063/1.5038773

2-dimensional electron gases (2DEGs) established in complex oxide interfaces have arrived at the heart of ongoing research in oxide electronics. Typically, these 2DEGs are formed due to the charge-transfer across two materials interfacing each other with atomic precision, effectively allowing an inherent gating of a material by a tailored built-in potential and giving rise to interfacial correlation effects and novel physical phenomena not accessible in the bulk.[1,2]

One central aspect for the general understanding of 2DEG formation, but also for the accessibility of 2DEGs with different properties (such as a tunable carrier density), is to achieve tailored stoichiometry of the capping layer acting as the donor layer and providing the electrons of the 2DEG.[3–6] As reported for $LaAlO_3/SrTiO_3$ (LAO/STO) heterostructures, the cation stoichiometry of the LAO-layer crucially affects the formation of the 2DEG,[7–9] as derived from the electronic reconstruction model, based on the net charge of atomic planes in polar oxides such as LAO.[3,4] In this context, the B-site-deficient case is of particular interest and controversy: It has been reported that B-site deficiency in the polar layer immediately leads to insulating interfaces, while A-site deficient compositions result in unattenuated 2DEG formation similar to the stoichiometric case.[7] Other reports, however, indicated

 

that both B-site rich and A-site rich compositions can result in 2DEG formation, albeit with reduced carrier density.[8,10]

In order to resolve this discrepancy, we utilize the 2DEG-system $NdGaO_3/SrTiO_3$ (NGO/STO). For this system, 2DEG formation[5,11–13] and defect-controllable transport properties and magnetism[12] have been reported. In contrast to its iso-ionic counterpart, LAO/STO, NGO/STO heterostructures bear the potential of tuning the cation stoichiometry of the polar NGO layer by variation of the growth temperature exploiting the volatility of gallium species.[5] Hence, in particular, B-site deficient (i.e., Ga-depleted) polar capping layers are easily obtained at an increased growth temperature.[5] As we demonstrate, we observe 2DEG formation even in significantly B-site deficient heterostructures, while charge transfer is significantly reduced as compared to the stoichiometric case. For experimental confirmation, we use angle-dependent hard x-ray photoelectron spectroscopy (HAXPES) of Ga and Nd core levels to obtain depth profiles of Ga non-stoichiometry in NGO thin films grown at different deposition temperatures. We reveal a Ga concentration gradient toward the surface and find that Ga-depletion (i.e., B-site-deficient composition) results in 2DEG formation with reduced carrier density, indicating diminished charge transfer in non-stoichiometric NGO/STO interfaces.

This result is inferred from a reduced $Ti^{3+}$ component in Ga-depleted samples as compared to a more stoichiometric case. Transport data moreover confirm confined metallicity at increased resistance in B-site deficient samples, with a major effect on the carrier density and sub-band occupation. By contrast, the electron mobility remains comparable, in accordance with a reduced amount of charge (electrons) being transferred across more non-stoichiometric interfaces. To explain this result, we propose an ionic reconstruction scenario based on the ionic compensation of cationic defects via accompanying anionic oxygen vacancies that form naturally in acceptor-doped transition metal oxides.[14–19]

PLD thin films were ablated from a single crystalline NGO target applying a laser fluence of 1.9 J/cm$^2$ at a repetition rate of 1 Hz and an oxygen pressure of $1 \times 10^{-4}$ mbar. $TiO_2$-terminated (100) STO single crystals were used as substrates. The growth temperature was 700 °C and 800 °C, obtaining close-to stoichiometric and Ga-deficient samples,[5] respectively. Reflection high energy electron diffraction (RHEED) indicated a layer-by-layer growth mode and allowed us to precisely control the NGO layer thickness to eight unit cells (≈3 nm, cf. Ref. 5). The samples were cooled down slowly in growth pressure at a rate of 10 °C/min to assure thermodynamic equilibration of the heterostructure.[20] In particular, the reoxidation of growth-induced oxygen vacancies is achieved, which typically takes place within 15-30 min at this growth pressure.[20] In this way, transport contributions caused by residual oxygen vacancies in the STO substrate are minimized. After growth, the samples were cut into two pieces, for transport measurements and spectroscopic characterization. For transport experiments, a mimicked Hall bar geometry was obtained by Al-wire bonding on a $1 \times 5$ mm$^2$-sized bar.[12] Hall and magneto resistance measurements were performed in a Physical Property Measurement System (PPMS, Quantum Design, $2 < T/\mathrm{K} < 300$, $-10 < B/\mathrm{T} < 10$). Field-dependent Hall data were anti-symmetrized and a two-channel model was applied to capture the non-linear field dependence of the Hall resistance, $R_{xy}$.

Hard x-ray photoelectron spectroscopy (HAXPES) experiments were performed at the GALAXIES beamline (SOLEIL, France) at $E_{\mathrm{photon}} = 2994.7$ eV and 3094.7 eV photon energy using a Si 111 monochromator and pass energies of 20 meV for Nd $3d_{5/2}$ and Ga $2p_{3/2}$ spectra and 100 meV for Ti $2p$ spectra. The overall energy resolution was 360 meV or better, as was regularly determined by the width of the Au Fermi edge. At photoelectron kinetic energies of 1878 eV (Ga $2p_{3/2}$) and 2015 eV (Nd $3d_{5/2}$) ($E_{\mathrm{photon}} = 2994.7$ eV), the inelastic mean free path (IMFP) for Ga $2p_{3/2}$ (Nd $3d_{5/2}$) photoelectrons is 3.11 nm (3.29 nm) in NGO, as calculated by the TPP2M code.[21] The IMFP well comparable to the NGO layer thickness allows us (1) to probe the buried STO substrate's Ti $2p$ core level with sufficient intensity at normal emission and (2) to employ angle-dependent HAXPES to probe the chemistry of the entire NGO layer all the way to the interface and with increasing surface sensitivity at increasing emission angle. Note that no transient changes of the recorded spectra were observed, indicating a negligible effect of beam damage.

The temperature-dependence of the sheet resistance ($R_s$) and field-dependent Hall resistance ($R_{xy}$) data obtained for samples grown at 700 °C and 800 °C are shown in Figs. 1(a) and 1(b). Both samples exhibit metallic resistance behavior. The resistance values for the high-temperature-grown

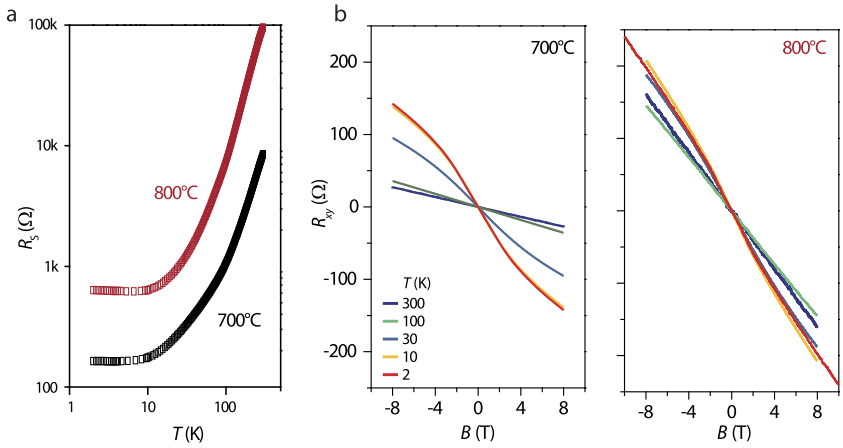


FIG. 1. Temperature dependent transport data for NGO/STO heterostructures grown at 700 °C and 800 °C, respectively. (a) Sheet-resistance at zero field, $R_{xx}$; (b) field-dependent Hall resistance, $R_{xy}$, demonstrating non-linear (2D) behavior at low temperatures ($\lesssim$30 K) for both samples.

sample (red), however, exceed the ones of the lower-temperature grown sample (black) over the entire temperature range. Both samples show non-linear field-dependence of the Hall effect at low temperatures ($\lesssim$30 K) attributed to multi-carrier transport[12,22,23] and reflecting the confined character of transport in both samples. In fact, the non-linear field behavior implies confined charge carriers in the vicinity of the interface, indicating an interfacial reconstruction taking place for both growth temperatures. The lifted degeneracy of d-orbitals responsible for multi-channel conduction relies on the confinement of charge carriers and an electric field distribution within the interface region. This strongly indicates electronic charge separation taking place at the interface, in contrast to a mere effect of oxygen ion transfer, where both electrons and oxygen vacancy defects reside on the STO side of the interface. The non-linear Hall effect was analyzed in a two-channel model revealing the typically observed low-density–high-mobility electron species and high-density–lower-mobility species. Figure 2 displays the corresponding sheet carrier densities, $n_i$ (a), and electron mobilities, $\mu_i$ (b), extracted from the data fit. Note that in both samples, an anomalous Hall component was also evident in the Hall coefficient as discussed in our earlier work (cf. Ref. 12). No significant dependence on growth temperature was observed. The extracted electron mobility ($\mu_i$) and carrier density ($n_i$)

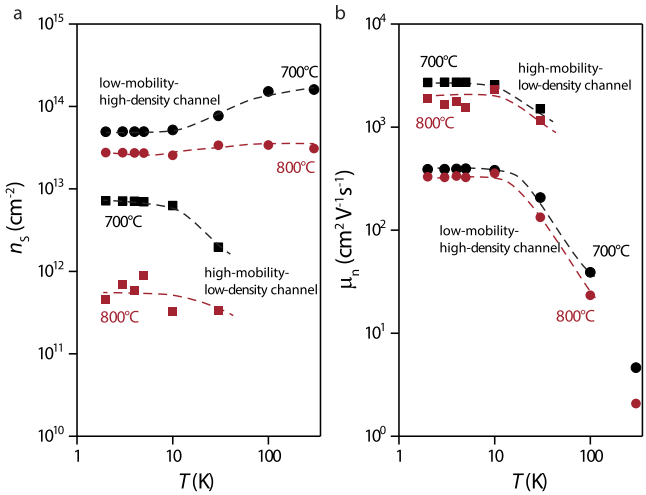


FIG. 2. (a) sheet carrier density, $n_i$, and (b) electron mobility, $\mu_i$, obtained from two-channel modeling of the non-linear Hall effect ($\lesssim$30 K). At 100 K and 300 K, the linear field-behavior of $R_{xy}$ is evaluated by standard single-channel transport ($R_{xy} = B/en_s$). Squares correspond to the high-mobility–low-density transport channel and circles correspond to the lower-mobility–high-density channel. The lines are guides to the eye.

values obtained from this analysis are not significantly affected by this anomalous contribution.[12] A detailed discussion of the two-channel analysis and anomalous Hall effect can be found in the supplementary material.

It becomes obvious that the increased sheet resistance of the high-temperature grown sample is caused primarily by a reduced carrier density, particularly in the high-mobility channel, dropping by one order of magnitude at 2 K. Similarly, the lower-mobility–high-density electron concentration is reduced. Moreover, at room temperature, the total carrier density is about one order of magnitude smaller in the high-temperature grown sample as compared to the lower-temperature one. (Note that the 700 °C sample shows a slight carrier freeze out as often observed in high carrier density 2DEGs, while the 800 °C sample shows a constant carrier density upon cooling.) By contrast, the mobility in both samples (and both transport channels) takes rather similar values, indicating that the reduced carrier density observed here dominantly originates from a reduced charge transfer, rather than from charge trapping in defect states,[24–26] which typically strongly affect electron mobility, too. The slight increase in mobility (factor of about 1.1–1.4) observed at a lower growth temperature is consistent with thermodynamic defect formation in oxides and their interfaces,[25,27] involving the formation of compensating cationic defects, and has been observed also for LAO/STO.[28] In particular, SrO segregation has been reported to occur under the applied growth conditions,[29] which goes hand in hand with the formation of Sr vacancies on the STO side of the interface. The main driving force for this, however, is the oxygen partial pressure applied during and after growth,[25] while an increased temperature has only a minor influence on the expected defect density.[12,24,25] Therefore, almost identical mobility observed in both samples investigated here indicates a major effect coming from the NGO capping layer properties, rather than from the intrinsic defect concentrations on the STO side of the interface.

The low occupation of the high-mobility channel ($\approx 5 \times 10^{11}$ cm$^{-2}$) and the reduced total carrier density ($\approx 3 \times 10^{13}$ cm$^{-2}$) below 10 K cause the weaker non-linearity observed in the Hall data (Fig. 1) and the concomitant scatter in the two-carrier analysis (Fig. 2). At reduced charge transfer in the high-temperature grown sample, moreover, the shape of the potential well,[23,30,31] and thus the inherent electric field distribution and position of the Fermi-level, is varied, which is consistent with an altered occupation of high-mobility and low-mobility channels (i.e., $n_1/n_2$-ratio).[22,32]

The confinement of the charge carriers at the NGO/STO interfaces as inferred from the non-linear Hall effect is corroborated by the presence of $Ti^{3+}$ probed by HAXPES at a take-off angle (TOA) of $\theta = 5°$ [close to normal emission, Fig. 3(a)]. The intensity of the $Ti^{3+}$ contribution observed as an intensity shoulder at 457.5 eV binding energy significantly decreases for the high-temperature grown sample as compared to the lower-temperature sample. Hence, the heterostructure showing the

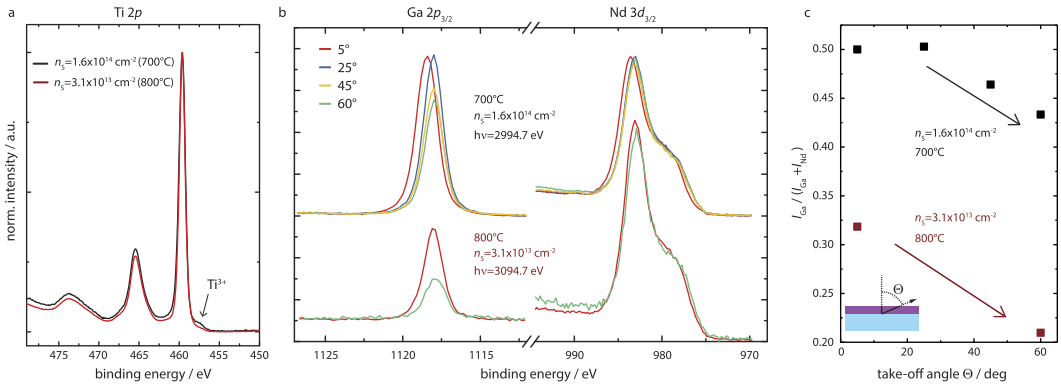


FIG. 3. HAXPES obtained for the NGO/STO heterostructures grown at 700 °C (top) and 800 °C (bottom). (a) Ti 2*p* spectra normalized to [0, 1] to compare the line shape and to reveal finite $Ti^{3+}$ contributions; (b) Ga 2*p* and Nd 3*d* core level spectra recorded for different take-off angles, $\theta$. The spectra have been normalized to the respective background intensity (i.e., the measured signal was divided by the respective pre-edge intensity to account for the footprint of the incoming beam varying with TOA). The top panel refers to the sample grown at 700 °C, the bottom panel to the sample grown at 800 °C. (c) Intensity ratio of the Ga core level with respect to the total intensity obtained from cation core level spectra. $I_{Ga}/(I_{Ga} + I_{Nd})$ was calculated from the peak area after background correction.

larger carrier density [700 °C, $n_S = 1.6 \times 10^{14}$ cm$^{-2}$ (black)] also shows a higher shoulder at the low binding energy side of the Ti $2p_{3/2}$ spectrum as compared to the lower carrier density sample [800 °C, $n_S = 3.1 \times 10^{13}$ cm$^{-2}$ (red) at 300 K].

In order to be distinguishable from the dominant $Ti^{4+}$ contribution, the $Ti^{3+}$ contribution is typically required to be of the order of a few percent of the total measured intensity signal,[33] which translates into a lower limit of the $Ti^{3+}$ concentration of order $\left[Ti^{3+}\right] \gtrsim 10^{20}$ cm$^{-3}$ within the STO probing volume. Hence, within a few nanometers, this volume carrier density adds to sheet carrier concentrations well comparable with the ones evident from transport measurements, indicating that in both samples, all carriers are located at the interface so that bulk contributions can be neglected. HAXPES hence confirms a reduced carrier concentration in the high-temperature grown sample as well as the confinement of the majority of electrons within the probing volume of a few nanometers from the interface.

In order to reveal the relation between reduced charge transfer and cation stoichiometry of the polar NGO capping layer, we employ the angular dependence of the Nd $3d_{5/2}$ and Ga $2p_{3/2}$ emission line intensity shown in Figs. 3(b) and 3(c) for $\theta = 5°$–$60°$ [corresponding to probing depths $3\lambda \cos(\theta)$ of about 10 nm–5 nm]. The measured signals were divided by the respective pre-edge intensities to account for the altered illumination area with varied TOA, allowing us to compare spectral intensities at different TOA. At larger emission angles, the spectral weight of the surface layer increases: At $\theta = 5°$, the entire NGO layer is probed within escape depths corresponding to one IMFP, while at $\theta = 60°$, the entire NGO layer is probed within escape depths corresponding to two IMPFs. Due to the exponential decay of the photoelectron intensity with escape depth, the photoelectron intensity emitted from, e.g., the 1st (2nd) unit cell of the NGO layer ($c_{NGO} = 0.386$ nm)[5] is approximately 18% (16%) at $\theta = 5°$ and 25% (20%) at $\theta = 60°$, relative to the total intensity, illustrating increased surface sensitivity at larger $\theta$-values. In all cases, however, the total signal is an average across the entire NGO layer (considering an information depth of 3IMFPs), all the way to the interface.

Experimentally, we observed on both samples that the Nd $3d_{5/2}$ line intensity remains almost constant for all take-off angles, while the Ga $2p_{3/2}$ intensity significantly drops off for higher TOA [Fig. 3(b)]. The line shape of both lines remains identical for all take-off angles, indicating no significant chemical changes for both species. The constant intensity of the Nd $3d_{5/2}$ line is a result of the fact that even for the largest TOA, the probing depth of the experiment is larger than the thickness of the NGO layer. Therefore, the amount of Nd-ions in the probed volume is constant, and for a homogeneous distribution of Nd across the layer, a constant intensity can be observed. By contrast, the diminished line intensity of Ga $2p_{3/2}$ for higher TOA indicates a concentration gradient being present in the Ga sublattice. As the measurements become more surface sensitive with increasing TOA, we interpret this as a concentration gradient parallel to the surface normal of the heterostructure and, thus, as a gradual Ga depletion toward the surface of the NGO layer.

These observations are displayed in a semi-quantitative manner in Fig. 3(c). The ratio of the normalized peak areas is displayed as $I_{Ga}/(I_{Ga} + I_{Nd})$ against TOA. Two observations are immediately obvious: (i) both samples show a lower $I_{Ga}/(I_{Ga} + I_{Nd})$ for higher TOA, i.e., less Ga at the surface, and (ii) the heterostructure grown at 800 °C (red squares) has a much lower overall amount of Ga. In addition, the Ga gradient in this heterostructure is more pronounced, since the decrease of the Ga $2p_{3/2}$ line intensity with TOA is larger. Thus, the surfaces of both films possess a lack of Ga, consistent with temperature controlled re-evaporation of Ga-species from the thin films.[5] Even more, the 800 °C-sample is severely substoichiometric and, in particular, B-site deficient. In fact, even at close-to-normal emission, the intensity ratio is not even close to the one observed for the 700 °C-sample. This severe Ga-deficiency observed for all TOAs in the 800 °C-sample indicates that the B-site deficiency induced during high temperature growth most likely penetrates the NGO layer all the way to the interface and is not only limited to the very surface region of the thin film. Moreover, as HAXPES delivers averaged data across the entire thin film, the large Ga-deficiency evident for the 800 °C sample indicates a strong gradient in stoichiometry toward the surface and a severe Ga-deficiency in the surface terminating layer, which may even result in an instability of the perovskite structure at the very surface.[5]

This compositional feature systematically coincides with the significantly reduced electron density observed both in Ti $2p$ HAXPES and transport. Hence, despite a significant B-site deficiency,

we still observe confined electron transport at the interfaces and, thus, a diminished but finite charge transfer across the interface. We note that $I_{Ga}/(I_{Ga} + I_{Nd})$ is calculated directly from the peak area after background correction. Hence, it does not directly translate into stoichiometry information, as relative sensitivity factors are not known at excitation energies applied in HAXPES. However, lab-based XPS (for which sensitivity factors were determined, cf. Ref. 5) indicated that a growth temperature of 700 °C results in close-to stoichiometric growth and hence Ga-deficient growth at 800 °C also in absolute values.

The experimental results are particularly notable as they reflect 2DEG formation in B-site deficient polar/non-polar oxide interfaces, which—following common sense—are expected to possess insulating interfaces.[7] Here, however, we observe 2DEG formation, confined to the NGO/STO interface, with comparable electron mobility at different overlayer stoichiometry, while the 2DEG's electron density decreases with increasing grade of non-stoichiometry of the polar NGO thin film. Hence, rather than observing a sharp transition to insulating behavior at B-site-deficient composition, we observe a diminished charge transfer across the interface.

For polar/non-polar oxide interfaces, charge transfer is typically understood in terms of the net charge of the atomic planes of the polar oxide layer,[3,4,7–9,30,34] as sketched in Fig. 4. For the stoichiometric case, alternating net charges of ±1 elementary charges (per areal unit cell, e/auc) give rise to a nominal charge transfer of 0.5 e/auc into the interface as sketched in Fig. 4(a). Here, we assume atomically sharp interfaces between STO substrate and the interfacing NGO layer.

For the non-stoichiometric case as elaborated here, it is now important to consider (1) how non-stoichiometry is accommodated in the polar oxide and (2) how compensating defects are distributed within the polar oxide layer. Due to their close-packed crystal structure, perovskite oxides do not form interstitial-type defects to accommodate excess cations. Therefore, cation deficiency results in the incorporation of acceptor-type cation vacancies. In the Ga-deficient this corresponds to the formation of Ga vacancies ($V'''_{Ga}$), which carry a three-fold negative net charge within the lattice.[14] In order to maintain charge neutrality, complex oxides naturally form positively charged oxygen vacancies ($V^{\bullet\bullet}_{O}$), rather than electron holes, to accommodate acceptor-type doping. Therefore, cation non-stoichiometry implies concomitant defect formation in the oxygen sublattice.[14,16,25,35] This co-doping process is widely employed to enhance and optimize ionic conductivity on oxygen ion conductors.[15] Therefore, Ga-deficient NGO layers are expected to crystallize as $NdGa_{1-y}O_{3-3y/2}$, where $y$ denotes the Ga-deficiency, accompanied by an oxygen-deficiency of $\delta = 3y/2$.

In this composition, the defect-containing NGO layers form charge neutral unit cells, independent of $y$ and independent of the actual location of defects within the lattice. However, the specific location

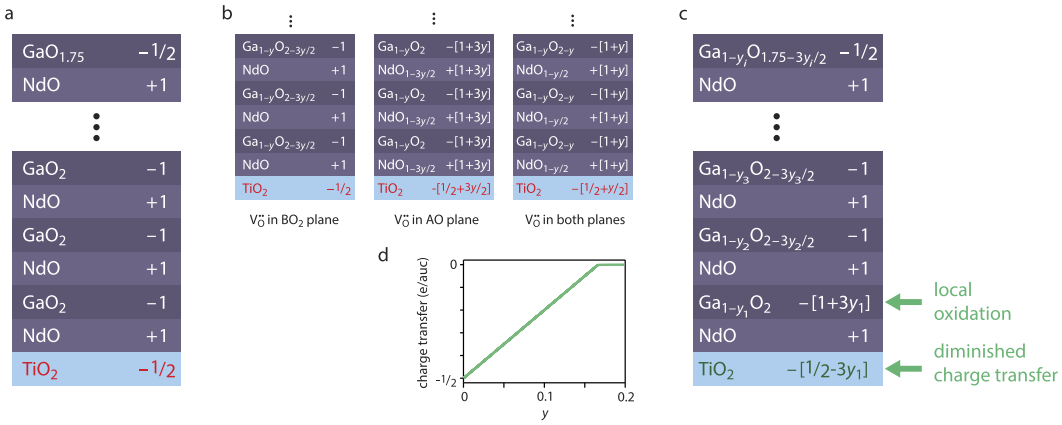


FIG. 4. Charge transfer at polar/non-polar oxide interfaces as derived from the net charges of atomic planes. (a) Stoichiometric case for NGO on (100) $TiO_2$-terminated STO; (b) non-stoichiometric case, assuming Ga vacancy defects being compensated by oxygen vacancies at different locations within the unit cell of the polar NGO layer; (c) lowered charge transfer into the interface achieved by an inhomogeneous distribution of oxygen vacancies within the lattice. In particular, oxidation of the interface-nearest $BO_2$-layer results in a diminished charge transfer that scales with increasing non-stoichiometry, $y$. (d) Scaling of expected charge transfer into the interface for different grades of B-site deficiency, $y$.

of defects within the unit cell is important when determining the net charge of (half unit cell) atomic layers, responsible for potential built-up in the polar oxide thin film: Clearly, Ga-vacancy defects are located in the negatively charged $B_{1-y}O_2$-planes, essentially *enhancing* the negative net charge of these atomic layers. Oxygen vacancies, however, may be formed in the AO-planes or in the $BO_2$-planes, thereby either *increasing* the positive net charge of the AO-layers or *decreasing* the negative net charge of $BO_2$-layers.

Locating both Ga-vacancy defects and compensating oxygen vacancies in the $BO_2$-planes only [Fig. 4(b1)] results in an unaffected net charge in both atomic planes, i.e., alternating stacking of ±1 e/auc. If this configuration was at play, one would hence expect no difference in charge transfer between the B-site deficient and stoichiometric case.

Locating compensating oxygen vacancies in AO-layers increases the net charges of single atomic planes even more [$\pm[1+3y]$ e/auc, Fig. 4(b2)]. Furthermore, homogeneous (or arbitrary) distribution of oxygen vacancies within both layers similarly results in an increase of net charge within the layers [e.g., $\pm[1+y]$ e/auc, cf. Fig. 4(b3)]. In these cases, potential built-up in the B-site deficient case would be even stronger than in the stoichiometric case, implying enhanced charge transfer across the interface and, thus, larger electron density in the 2DEG of B-site deficient heterostructures. This is the opposite behavior as derived for A-site deficient heterostructures, where cationic defects in the positively charged $AO^+$-layer result in lowered net charges of single atomic planes in the polar layer.[8]

In this picture, scenario b1 is energetically the most favorable, as it results in minimum potential energy with increasing NGO layer thickness. Furthermore, this scenario also sets a lower limit for achievable net charges of atomic planes in B-site deficient composition. Hence, the reduced carrier density observed here cannot be explained in these "homogeneous" scenarios. Rather, inhomogeneous defect profiles have to be considered to understand the observed behavior. Local inhomogeneity of defect distributions has already been considered in the literature (1) to explain the missing thermal stability in nominally polar $\gamma$-$Al_2O_3$/STO[6,9] and (2) to explain insulating interfaces in Al-deficient LAO/STO heterostructures:[7] Here, a scenario of spontaneous formation and migration of 1/6 Al-vacancies per auc in the interfacial $AlO_2$-layer was derived. These lead to insulating interfaces—independent of the actual grade of non-stoichiometry of the polar capping layer.

As we argue, however, the presence of intrinsic (growth-induced) B-site vacancies allows an alternative explanation based on a redistribution of oxygen vacancies, which in oxides are by far more mobile as compared to the cations.[18,19] For this, we start from the configuration of a defect-buffered NGO layer, in which oxygen vacancies are located in the $Ga_{1-y}O_{2-3y/2}$ atomic planes and which reflects the lowest energy configuration among the homogenous defect distributions displayed in Fig. 4(b). Full oxidation of the interface-nearest atomic layer ($Ga_{1-y}O_2$) readily results in a reduced potential built-up in the polar NGO layer and, hence, in a corresponding charge transfer of only $[0.5-3y]$ e/auc required to avoid a diverging potential [Fig. 4(c)]. For a given $y$, one can hence expect charge transfer that deviates from 0.5 e/auc. In fact, the interface-oxidation model delivers a reduced charge carrier density for finite Ga-deficiency (i.e., $y > 0$) that further decreases with increasing grade of non-stoichiometry [Fig. 4(d)]. Eventually, this leads to fully insulating behavior for large non-stoichiometry (when $y$ approaches 1/6), thus reproducing the results of Ref. 7. The threshold for insulating behavior may deviate from this exact number when additional charge compensating processes such as lattice distortions and polarization apply.[36] A gradual change in cation stoichiometry as observed in angle-dependent HAXPES can easily be understood in this picture by assigning individual Ga-deficiency, $y_i$, for each unit cell across the thin film [cf. Fig. 4(c)]: In this case, $y_1$ in the interface-nearest unit cell is the relevant number, which determines the amount of required charge transfer, while subsequent unit cells follow the common ±1-scheme. In this view, the interface-nearest unit cells of the capping layer determine the properties of the interface. Even phase instability in the surface terminating layer may not be crucial for interface reconstruction, provided that the interface-nearest unit cells maintain stoichiometry within the limit of $y_i < 0.16$, in order to provide sufficient potential built-up.

Our reconstruction employs redistribution of oxygen ions only and, hence, avoids the spontaneous formation and redistribution of additional B-site cation vacancies,[7,9] which have a much

lower mobility than oxygen vacancies, and avoids the kinetically even more unfavorable anti-site defects.[7,37] The smooth transition from 2DEG formation to 2DEG formation with diminished charge transfer to insulating behavior with increasing grade of non-stoichiometry deriving from our model is furthermore fully consistent with the experimental results of our study as well as the ones reported in Ref. 8.

The proposed oxidation of interface-near atomic layers implies the redistribution of oxygen vacancies away from the interface and hence the accumulation of oxygen vacancies at the surface of the oxide layer (as global charge neutrality needs to be maintained). The driving force for this redistribution of oxygen vacancies within the polar layer is the inherent necessity of a positive net charge accumulated at the surface of the polar oxide (at first, assigned to electron holes at the surface,[4] but nowadays assigned to surface oxygen vacancy formation).[37] Cation substoichiometry in the NGO layer provides already a sufficient reservoir of oxygen vacancy defects, promoting charge separation by redistribution, rather than spontaneous formation of defects.

In conclusion, we have demonstrated 2DEG formation in strongly B-site deficient polar/non-polar oxide interfaces, showing confined electron transport with electron mobility comparable to more stoichiometric samples. Non-stoichiometric samples are found to possess reduced electron densities and thus a diminished charge transfer across the interface, as evident from low temperature Hall measurements, Ti 2*p* spectroscopy, and angle dependent HAXPES of Ga and Nd core levels. As we suggest, atomic redistribution of oxygen vacancies allows for 2DEG formation with diminished charge transfer in the B-site deficient case and—in the limit of strong B-site deficiency—explains the insulating behavior observed in the literature.

Owing to the almost unchanged electron mobility, stoichiometry effects within the polar capping layer reflect one routine for obtaining tailored 2DEG densities, without losing performance, in complex oxide heterostructures. Our study moreover demonstrates the huge impact of atomic reconfiguration of defects on the single unit cell level for the properties of nanoscale oxide electronic devices.

See supplementary material for details on the fitting procedure of non-linear Hall data and a discussion of anomalous Hall effect contributions.


[1] H. Y. Hwang, Y. Iwasa, M. Kawasaki, B. Keimer, N. Nagaosa, and Y. Tokura, Nat. Mater. **11**, 103 (2012).
[2] D. G. Schlom and J. Mannhart, Nat. Mater. **10**, 168 (2011).
[3] A. Ohtomo and H. Y. Hwang, Nature **427**, 423 (2004).
[4] N. Nakagawa, H. Y. Hwang, and D. A. Muller, Nat. Mater. **5**, 204 (2006).
[5] F. Gunkel, K. Skaja, A. Shkabko, R. Dittmann, S. Hoffmann-Eifert, and R. Waser, Appl. Phys. Lett. **102**, 071601 (2013).
[6] F. Gunkel, S. Hoffmann-Eifert, R. A. Heinen, D. V. Christensen, Y. Z. Chen, N. Pryds, R. Waser, and R. Dittmann, ACS Appl. Mater. Interfaces **9**, 1086 (2017).
[7] M. P. Warusawithana, C. Richter, J. A. Mundy, P. Roy, J. Ludwig, S. Paetel, T. Heeg, A. A. Pawlicki, L. F. Kourkoutis, M. Zheng, M. Lee, B. Mulcahy, W. Zander, Y. Zhu, J. Schubert, J. N. Eckstein, D. A. Muller, C. S. Hellberg, J. Mannhart, and D. G. Schlom, Nat. Commun. **4**, 2351 (2013).
[8] H. K. Sato, C. Bell, Y. Hikita, and H. Y. Hwang, Appl. Phys. Lett. **102**, 251602 (2013).
[9] D. Christensen and A. Smith, Appl. Surf. Sci. **423**, 887 (2017).
[10] E. Breckenfeld, N. Bronn, J. Karthik, A. R. Damodaran, S. Lee, N. Mason, and L. W. Martin, Phys. Rev. Lett. **110**, 196804-1 (2013).
[11] E. Di Gennaro, U. S. di Uccio, C. Aruta, C. Cantoni, A. Gadaleta *et al.*, Adv. Opt. Mater. **1**, 834 (2013).
[12] F. Gunkel, C. Bell, H. Inoue, B. Kim, A. G. Swartz, T. A. Merz, Y. Hikita, S. Harashima, H. K. Sato, M. Minohara, S. Hoffmann-Eifert, R. Dittmann, and H. Y. Hwang, Phys. Rev. X **6**, 031035 (2016).
[13] A. Annadi, A. Putra, Z. Q. Liu, X. Wang, K. Gopinadhan, Z. Huang, S. Dhar, T. Venkatesan, and Ariando, Phys. Rev. B **86**, 085450 (2012).
[14] D. M. Smyth, *The Defect Chemistry of Metal Oxides* (Oxford University Press, New York, 2000).
[15] S. J. Skinner and J. A. Kilner, Mater. Today **6**, 30 (2003).
[16] R. Moos and K. H. Haerdtl, J. Am. Ceram. Soc. **80**, 2549 (1997).
[17] T. L. Nguyen, Solid State Ionics **130**, 229 (2000).
[18] T. Ishihara, H. Matsuda, M. A. bin Bustam, and Y. Takita, in *Proceedings of the 10th International Conference on Solid State Ionics* [Solid State Ionics **86-88**(Part 1), 197 (1996)].
[19] T. Ishihara, H. Matsuda, and Y. Takita, J. Am. Chem. Soc. **116**, 3801 (1994).
[20] C. Xu, C. Bäumer, R. A. Heinen, S. Hoffmann-Eifert, F. Gunkel, and R. Dittmann, Sci. Rep. **6**, 022410 (2016).
[21] S. Tanuma, C. Powell, and D. Penn, Surf. Interface Anal. **21**, 165 (1994).
[22] A. Joshua, J. Ruhman, S. Pecker, E. Altman, and S. Ilani, Proc. Natl. Acad. Sci. U. S. A. **110**, 9633 (2013).
[23] C. Bell, S. Harashima, Y. Kozuka, M. Kim, B. G. Kim, Y. Hikita, and H. Y. Hwang, Phys. Rev. Lett. **103**, 226802 (2009).
[24] F. Gunkel, P. Brinks, S. Hoffmann-Eifert, R. Dittmann, M. Huijben, J. E. Kleibeuker, G. Koster, G. Rijnders, and R. Waser, Appl. Phys. Lett. **100**, 52103-1 (2012).

[25] F. Gunkel, R. Waser, A. H. H. Ramadan, R. A. D. Souza, S. Hoffmann-Eifert, and R. Dittmann, Phys. Rev. B **93**, 245431 (2016).
[26] F. Gunkel, S. Wicklein, P. Brinks, S. Hoffmann-Eifert, M. Huijben, G. Rijnders, R. Waser, and R. Dittmann, Nanoscale **7**, 1013 (2015).
[27] R. Meyer, A. F. Zurhelle, R. A. D. Souza, R. Waser, and F. Gunkel, Phys. Rev. B **94**, 115408 (2016).
[28] A. Fete, C. Cancellieri, D. Li, D. Stornaiuolo, A. D. Caviglia, S. Gariglio, and J.-M. Triscone, Appl. Phys. Lett. **106**, 051604 (2015).
[29] U. Treske, N. Heming, M. Knupfer, B. Buechner, A. Koitzsch, E. Di Gennaro, U. S. di Uccio, F. M. Granozio, and S. Krause, APL Mater. **2**, 012108 (2014).
[30] F. Gunkel, R. A. Heinen, S. Hoffmann-Eifert, L. Jin, C. Jia, and R. Dittmann, ACS Appl. Mater. Interfaces **9**, 010888 (2017).
[31] M. Minohara, Y. Hikita, C. Bell, H. Inoue, M. Hosoda, H. K. Sato, H. Kumigashira, M. Oshima, E. Ikenaga, and H. Y. Hwang, Sci. Rep. **7**, 9516 (2017).
[32] A. F. Santander-Syro, O. Copie, T. Kondo, F. Fortuna, S. Pailhes, R. Weht, X. G. Qiu, F. Bertran, A. Nicolaou, A. Taleb-Ibrahimi, P. Le Fevre, G. Herranz, M. Bibes, N. Reyren, Y. Apertet, P. Lecoeur, A. Barthelemy, and M. J. Rozenberg, Nature **469**, 189 (2011).
[33] M. Sing, G. Berner, K. Goss, A. Mueller, A. Ruff, A. Wetscherek, S. Thiel, J. Mannhart, S. A. Pauli, C. W. Schneider, P. R. Willmott, M. Gorgoi, F. Schaefers, and R. Claessen, Phys. Rev. Lett. **102**, 176805-1 (2009).
[34] M. Reinle-Schmitt, C. Cancellieri, D. Li, D. Fontaine, M. Medarde *et al.*, Nat. Commun. **3**, 932 (2012).
[35] F. Gunkel, S. Hoffmann-Eifert, R. Dittmann, S. Mi, C. Jia, P. Meuffels, and R. Waser, Appl. Phys. Lett. **97**, 012103 (2010).
[36] C. Cantoni, J. Gazquez, F. M. Granozio, M. P. Oxley, M. Varela, A. R. Lupini, S. J. Pennycook, C. Aruta, U. S. di Uccio, P. Perna, and D. Maccariello, Adv. Mater. **24**, 3952 (2012).
[37] L. Yu and A. Zunger, Nat. Commun. **5**, 5118 (2014).